Int. J. Heat Mass Transfer. Vol. 36, No. 9, pp. 2417–2427, 1993
Printed in Great Britain

0017-9310/93 $6.00 + 0.00
Pergamon Press Ltd

Buoyant-thermocapillary instabilities in medium-Prandtl-number fluid layers subject to a horizontal temperature gradient

PATRICE M. PARMENTIER, VINCENT C. REGNIER and GEORGY LEBON
Institute of Physics, Liège University, B5, Sart-Tilman B-4000 Liège, Belgium

(*Received* 11 *June* 1992)

Abstract—Coupled buoyant and thermocapillary instabilities in a fluid layer of infinite horizontal extent bounded below by a rigid plane and above by a free flat surface and submitted to a temperature gradient are investigated. A general 3D mathematical formulation is used to determine the linearized perturbated equations of the steady state induced by the temperature gradient. Numerical results are obtained in the case of a horizontal temperature gradient, lower and upper surfaces are adiabatically isolated and the range of variation of the Prandtl number is selected as $[10^{-2}, 10]$. The presence of travelling rolls is exhibited. The results display three kinds of behaviour according to the values taken by the Prandtl number: (a) $4 \times 10^{-3} < Pr < 0.4$, (b) $0.4 < Pr < 2.6$ and (c) $Pr > 2.6$.

1. INTRODUCTION

COUPLED effects of buoyancy and thermocapillarity in an infinite horizontal layer of fluid submitted to a temperature gradient are studied. This problem is generally referred to as the Bénard–Marangoni problem. The imposed temperature gradient can take two privileged directions: either a pure vertical one or a pure horizontal one. Nield [1] was the first to determine the instability thresholds in the case of a quiescent fluid of horizontal infinite extent, subjected to a vertical temperature gradient. The presence of a horizontal temperature gradient raises several additional difficulties. First, the rest state is not the solution of the balance equations and therefore a preliminary study must be realized to determine the basic temperature and velocity profiles [2]. The usual linear perturbation techniques can then be used to find the thresholds of the first instability mode. The second difficulty, the theorem of exchange of stability, has not been proved for a horizontal temperature gradient: experimental and numerical simulations show even the presence of oscillatory regimes [3–10]. Thirdly, in the case of a horizontal temperature gradient, the instability threshold depends strongly on the Prandtl number while it is independent of this parameter when a vertical temperature difference is acting [1]. A linear analysis of instabilities in thermocapillary liquid layers submitted to a horizontal temperature gradient was performed by Smith and Davis [6]. They identify two mechanisms of instabilities: the first is occurring as a consequence of the energetic balance between heat conduction and heat convection at the free surface, the second is related to the mechanical transfer of momentum from the basic state to the disturbance through the Reynolds stress in the layer; this second effect is particularly important in the presence of free surface deformations and occurs principally at small Prandtl numbers ($Pr < 10^{-1}$) [7]. Smith and Davis [6] did not examine the influence of buoyancy. Thermogravitational effects in layers submitted to a horizontal temperature gradient were studied by Hart [11], Laure and Roux [5, 12] for Prandtl numbers lower than 1. In the particular case of two adiabatic horizontal surfaces, these authors found an asymptotic value for the critical Rayleigh number at $Pr = 0.40$. But they did not look for an eventual bifurcation point situated beyond $Pr = 0.40$. To our knowledge, the only theoretical contribution to the study of coupled thermocapillarity and buoyancy instabilities in layers submitted to a horizontal temperature gradient is a paper by Ben Hadid *et al.* [8]. These authors were essentially interested by the study of liquid metals for which the Prandtl numbers are very small ($Pr \leqslant 5 \times 10^{-2}$). Moreover, they used different thermal boundary conditions for the basic and the disturbed states: the free surface was adiabatic for the basic state and perfectly heat conducting for disturbances.

The present paper concerns the problem of coupled thermocapillary and buoyancy effects in liquids with Prandtl number values ranging from 10^{-2} to 10. These Prandtl numbers correspond to current fluids: for example $Pr_{(\text{acetone})} = 4.24$ and $Pr_{(\text{water})} = 7$. A general 3D mathematical formulation is used. After recalling the relevant governing balance equations and boundary conditions in Section 2, the velocity and temperature profiles of the basic state are established in Section 3: the imposed temperature gradient is general in the sense it has simultaneously a horizontal and a vertical component. In Section 4, a linear stability

NOMENCLATURE

b	dimensionless heat exchange coefficient
B	Biot number, $h\,d\,K^{-1}$
C_p	specific heat
C_i	physical constants ($i = 1$–4)
c	phase speed
C	physical constant
d	height of the fluid layer
D	non-dimensional z-coordinate derivative, d/dz
Gr	Grashof number, $g\alpha_T\beta_T\,\mathrm{d}^4\nu^{-2}$
h	heat exchange coefficient
k	overall wave number
K	thermal conductivity
M	mass flux
Ma	Marangoni number, $\gamma\beta_T d^2\kappa^{-1}\nu^{-1}\rho_0^{-1}$
p	dimensionless pressure
Pr	Prandtl number, $\nu\kappa^{-1}$
$Q_{h,v}$	multiplicative factors of characteristic temperature gradient
Ra	Rayleigh number, $g\alpha_T\beta_T d^4\nu^{-1}\kappa^{-1}$
Re	Reynolds number, $\gamma\beta_T d^2\nu^{-2}\rho_0^{-1}$
s	complex stability parameter
t	dimensionless time
T	dimensionless temperature
u	dimensionless velocity field
u, v, w	dimensionless x-, y-, z-velocity components
x, y, z	dimensionless space coordinates.

Greek symbols

α_T	coefficient of volumic expansion
α, β	disturbance wave numbers in x-, y-axis
β_T	characteristic temperature gradient
γ	rate of change of surface tension with temperature
∂_t	partial time derivative operator
$\partial_{x,y,z}$	partial space derivative with respect to x, y and z
κ	thermal diffusivity
λ	complex eigenvalue
μ	dynamic viscosity
ν	kinematic viscosity
∇	nabla operator
ρ	density
σ	surface tension
$\Phi_{1,2}$	complex differential operators
Ψ	direction of disturbance propagation.

Subscripts

_	basic state quantity
0	reference quantity
I	imaginary part
l	lower rigid surface
R	real part
u	free upper surface.

Superscripts

∞	surrounding quantity
$'$	perturbation variable
*	perturbation amplitude
c	critical value.

analysis is presented for the particular case of a horizontally imposed temperature gradient at the upper surface of a layer enclosed between two adiabatically isolated planes. The flow is considered as being in a slot which induces a velocity profile usually referred as 'return flow' [4–6, 11, 13]. Final comments and comparison with other works are found in Section 5.

2. MATHEMATICAL FORMULATION

Consider a fluid layer of infinite horizontal extent confined between a rigid plane $z = 0$ and a free surface whose height is located at $z = d$. Since the deflection of the free surface is generally small [6, 7, 9, 13], we assume in this note that the free surface is flat. Cartesian coordinates are used with the origin at the rigid lower plane and the x, y axis oriented in the directions given by Fig. 1.

The fluid is Newtonian and incompressible with density given by

$$\rho = \rho_0[1-\alpha_T(T-T_0)] \qquad (1)$$

where ρ_0 is the density at temperature T_0 and α_T the constant coefficient of volumic expansion. Boussinesq's approximation is taken for granted; accordingly the dynamic viscosity μ, the specific heat C_p, and the thermal conductivity K are constant while the rate of production of heat by internal friction is neglected.

The free upper surface is submitted to a surface tension σ, whose equation of state is given by

$$\sigma = \sigma_0-\gamma(T-T_0) \qquad (2)$$

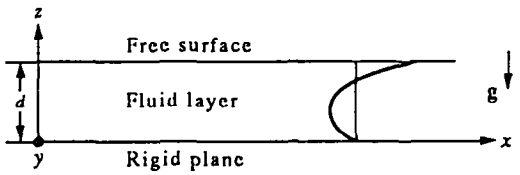

FIG. 1. The geometrical configuration: the curve gives the basic velocity profile, referred to as the return flow solution.

where σ_0 is the surface tension at temperature T_0, γ the constant rate of change of surface tension with temperature (γ is positive for most current liquids).

For convenience, the variables are expressed in dimensionless form. Distances are scaled by the thickness of the layer d; the velocity vector $\mathbf{u} = (u, v, w)$, time t, pressure p, temperature difference and surface tension σ are scaled by κd^{-1}, κd^2, $\kappa\nu\rho_0 d^{-2}$, $\beta_T d$ and σ_0 respectively, where $\kappa \equiv KC_p^{-1}\rho_0^{-1}$ is the diffusivity, $\nu \equiv \mu\rho_0^{-1}$ the kinematic viscosity and β_T a characteristic temperature gradient whose physical meaning will be specified later when the boundary conditions are established. The following dimensionless numbers are also introduced:

$$Pr \equiv \nu\kappa^{-1}, \quad Ra \equiv g\alpha_T\beta_T d^4\kappa^{-1}\nu^{-1}$$

$$Ma \equiv \gamma\beta_T d^2\kappa^{-1}\nu^{-1}\rho_0^{-1}, \quad B \equiv hdK^{-1}.$$

Pr is the Prandtl number, Ra the Rayleigh number, Ma the Marangoni number and B the Biot number, with h the thermal surface conductance. Some authors refs. [5, 7–12] use different dimensionless numbers as Reynolds and Grashof numbers defined respectively by

$$Re \equiv Ma\,Pr^{-1}, \quad Gr \equiv Ra\,Pr^{-1}.$$

The Rayleigh number is representative of the buoyancy effect while the Marangoni number describes more particularly the thermocapillarity effects, Grashof and Reynolds numbers are representative of the same effects respectively, but are divided by the Prandtl number. Within Boussinesq's approximation, the governing dimensionless equations are:

the continuity equation:

$$\nabla\cdot\mathbf{u} = 0 \tag{3}$$

the Navier–Stokes equation:

$$\partial_t\mathbf{u} + \mathbf{u}\cdot\nabla\mathbf{u} = Pr(-\nabla p + Ra\,T\mathbf{e}_z + \nabla^2\mathbf{u}) \tag{4}$$

the energy equation:

$$\partial_t T + \mathbf{u}\cdot\nabla T = \nabla^2 T. \tag{5}$$

$\nabla = (\partial_x, \partial_y, \partial_z)$ is the nabla operator, ∂_t and ∂_x, ∂_y, ∂_z stand for the partial time derivative and the partial space derivatives with respect to x, y, z respectively; $\mathbf{e}_z$ is the unit vector in z-direction.

The fluid layer is submitted to a temperature gradient with an arbitrary orientation with regard to the fluid layer. Let us denote by $Q_h\beta_T K$ and $Q_v\beta_T K$ the horizontal-x and vertical-z components of the imposed heat flux, written in dimensional form; Q_h and Q_v are multiplicative dimensionless factors while β_T is the common factor appearing in both components of the imposed heat flux. In order that the Rayleigh and Marangoni numbers correspond to the classical ones in the cases of pure horizontally or vertically imposed gradients, Q_h and Q_v are normalized by

$$(Q_v^2 + Q_h^2)^{1/2} = 1. \tag{6}$$

The boundary conditions are:

On the rigid plane $z = 0$:

$$u = v = w = 0 \tag{7}$$

$$\partial_z T = B_l(T - T_l^\infty) + Q_v. \tag{8}$$

Equation (7) expresses the no-slip condition while equation (8) is the general heat transfer condition: subscript 'l' refers to the lower plane, B_l is the Biot heat transfer coefficient, and T^∞ is the temperature of the external surroundings.

On the free top plane $z = 1$:

$$\partial_z u = -Ma\partial_x T, \quad \partial_z v = -Ma\partial_y T \tag{9}$$

$$w = 0 \tag{10}$$

$$-\partial_z T = B_u(T - T_u^\infty) + Q_v. \tag{11}$$

Equations (9) and (10) are the boundary conditions for a non-deformable flat surface with a temperature-dependent surface tension. In equation (11) subscript 'u' refers to the upper free surface. It is noted that Q_h and Q_v are arbitrary parameters that can be given any value between 0 and 1.

3. THE BASIC STATE

As soon as the imposed temperature gradient has non-zero horizontal component, i.e. $Q_h \neq 0$, a convective motion sets in. In contrast with the classical Bénard–Marangoni problem, with a vertical component temperature gradient, the basic steady state is not a state of rest.

Because of the hypothesis of infinite horizontal extent the only non-zero component of velocity is u which, by continuity, depends only on the z-coordinate, refs. [2, 4–6, 11, 13]. After eliminating the pressure, the momentum and energy equations in the steady state are:

$$\partial_{zzz}\underline{u} = Ra\,\partial_x\underline{T} \tag{12}$$

$$\underline{u}\partial_x\underline{T} = \partial_{zz}\underline{T}. \tag{13}$$

This situation is referred to as the 'basic state' and the corresponding variables are underlined.

The relevant boundary conditions are:

at $z = 0$

$$\underline{u} = 0 \tag{14}$$

$$\partial_z\underline{T} = B_l(\underline{T} - T_l^\infty) + Q_v \tag{15}$$

at $z = 1$

$$\partial_z\underline{u} = -Ma\,\partial_x\underline{T} \tag{16}$$

$$-\partial_z\underline{T} = B_u(\underline{T} - T_u^\infty) + Q_v. \tag{17}$$

Finally, the steady state must satisfy the global condition:

$$\partial_x \underline{T} = -Q_h. \tag{18}$$

Moreover $T_l^\infty - T_u^\infty = Q_v$ so that Q_v must be viewed as an external vertical heat flux which is superimposed on the vertical heat flux resulting from the application of the horizontal temperature gradient.

The conservation of mass can be expressed by means of the condition

$$M = \int_0^1 \int_0^1 u \, dy \, dz \quad \forall x \tag{19}$$

where M is the mass of liquid crossing a unit square area perpendicular to the x-axis per unit time. In the particular case of a zero-mass flux ($M = 0$), the solution corresponds to a Hadley circulation in a slot for which the assumptions $v = w = 0$ are not verified near the vertical walls. Nevertheless, it was shown by Sen and Davis [13] that the relevant region wherein a return motion is observed has a dimension of the order $O(d/l)$ with l defined as the slot length. Since the present analysis concerns only shallow cavities for which $d/l \ll 1$, our asymptotic solution will tend towards the exact solution for vanishing d/l.

The solutions of the basic velocity and temperature profiles are given by:

$$\underline{u} = -Q_h Ra\, z^3/3! + C_1 z^2/2! - C_2 z, \tag{20}$$

$$\underline{T} = Q_h\{Q_h Ra\, z^5/5! - C_1 z^4/4! + C_2 z^3/3! + C_3[1 - b_l(1-z)](b_l - b_l b_u + b_u) - 1\} - Q_v z - Q_h x \tag{21}$$

under the conditions that

$$T_l^\infty = -Q_h x, \quad T_u^\infty = -Q_h x - Q_v. \tag{22}$$

The particular choice of equation (22) for the external surroundings temperatures is necessary to obtain a steady solution. The undefined quantities C_1, C_2, C_3, b_l and b_u appearing in equations (20) and (21) are given by

$$C_1 = 3/2 Q_h Ma + 5/8 Q_h Ra - 3M \tag{23}$$

$$C_2 = 1/2 Q_h Ma + 1/8 Q_h Ra - 3M \tag{24}$$

$$C_3 = -b_u Q_h (1/48 Ma + 1/320 Ra) + M(1 - 5/8 b_l) \tag{25}$$

$$b_u = B_u(1 + B_u)^{-1} \tag{26}$$

$$b_l = B_l(1 + B_l)^{-1}. \tag{27}$$

The use of parameter b rather than Biot's number B is justified by the property that the domain of variation of b is [0, 1] for any positive value of B: $b = 0$ corresponds to an adiabatic boundary condition and $b = 1$ to a perfectly heat conduction surface.

In the case $b_l = b_u = 0$, equations (12) and (13) admit a solution only for a zero-mass flux M since two adiabatic surfaces prevent any heat dissipation through these surfaces. Under these conditions, the temperature profile equation (21) simplifies as

$$\underline{T}(b_l = b_u = 0; M = 0) = Q_h(Q_h Ra\, z^5/5! - C_1 z^4/4! + C_2 z^3/3!) - Q_v z - Q_h x + C_4 \tag{28}$$

wherein C_4 is an arbitrary constant whose value is not relevant because, as will be shown in next section, $\underline{T}$ will appear only in the form of derivatives.

4. A LINEAR PERTURBATION ANALYSIS

Our aim is to study the stability of the basic state under infinitesimally small disturbances. The general solution of the problem will be written as

$$(u, v, w, p, T) = (\underline{u}, \underline{v}, \underline{w}, \underline{p}, \underline{T}) + (u', v', w', p', T') \tag{29}$$

wherein primes denote perturbations. Introducing equation (4.1) in equations (2.3–2.5) and dropping non-linear terms in the perturbations leads to:

$$\partial_x u' + \partial_y v' + \partial_z w' = 0 \tag{30}$$

$$\partial_t u' + \underline{u}\partial_x u' + w'\partial_z \underline{u} = Pr(-\partial_x p' + \nabla^2 u') \tag{31}$$

$$\partial_t v' + \underline{u}\partial_x v' = Pr(-\partial_y p' + \nabla^2 v') \tag{32}$$

$$\partial_t w' + \underline{u}\partial_x w' = Pr(-\partial_z p' + \nabla^2 w' + RaT') \tag{33}$$

$$\partial_t T' + \underline{u}\partial_x T' + u'\partial_x \underline{T} + w'\underline{T} = \nabla^2 T' \tag{34}$$

with the boundary conditions

at $z = 0$

$$u' = v' = w' = 0 \tag{35}$$

$$-(1 - b_l)\partial_z T' + b_l T' = 0 \tag{36}$$

at $z = 1$

$$w' = 0 \tag{37}$$

$$\partial_z u' = -Ma\, \partial_x T' \tag{38}$$

$$\partial_z v' = -Ma\, \partial_y T' \tag{39}$$

$$(1 - b_u)\partial_z T' + b_u T' = 0. \tag{40}$$

According to the normal mode technique, we seek solutions of the form:

$$(u', v', w', p', T') = [u^*(z), v^*(z), w^*(z), p^*(z), T^*(z)]\, e^{i(\alpha x + \beta y - st)} \tag{41}$$

where an asterisk refers to the amplitudes and s is the complex stability parameter

$$s = s_R + i s_I \tag{42}$$

wherein s_I measures the growth rate of the disturbance, α and β are disturbance wave numbers in the x- and y-axis, respectively; $\alpha = 0$ corresponds to longitudinal rolls with axes aligned in the direction the bulk flow, $\beta = 0$ to transverse rolls with axes normal to the flow. The direction of propagation of the disturbance with regard to the x-axis is measured by means of angle Ψ defined as

$$\Psi = \tan^{-1}(\beta/\alpha). \tag{43}$$

The corresponding phase speed is given by

$$c = s_R k^{-1} \tag{44}$$

where k stands for

$$k = (\alpha^2+\beta^2)^{1/2}. \tag{45}$$

At marginal stability, the growth rate s_I of the perturbation is zero, so that $s = s_R$. Substitution of equation (41) in equations (30)–(40) results in the following differential equations for the disturbance amplitudes:

$$Dw^* + i\alpha u^* + i\beta v^* = 0 \tag{46}$$

$$\Phi_1 u^* = i\alpha Pr\, p^* + w^* D\underline{u} \tag{47}$$

$$\Phi_1 v^* = i\beta Pr\, p^* \tag{48}$$

$$\Phi_1 w^* = Pr\, Dp^* - Pr\, Ra\, T^* \tag{49}$$

$$\Phi_2 T^* = u^* \partial_x \underline{T} + w^* \partial_z \underline{T} \tag{50}$$

where D stands for $D \equiv \mathrm{d}/\mathrm{d}z$ while Φ_1 and Φ_2 are given by

$$\Phi_1 \equiv Pr(D^2-k^2) - i\alpha\underline{u} + is$$

$$\Phi_2 \equiv D^2 - k^2 - i\alpha\underline{u} + is.$$

After elimination of the pressure and the v^*-component of the velocity from the continuity equation (46), it is found that:

$$\Phi_1(D^2-k^2)w^* = -i\alpha D(D\underline{u}w^*) + k^2\, Pr\, Ra\, T^* \tag{51}$$

$$\Phi_1(k^2u^* - i\alpha Dw^*) = \beta^2 w^* D\underline{u} \tag{52}$$

$$\Phi_2 T^* = u^* \partial_x \underline{T} + w^* \partial_z \underline{T} \tag{53}$$

while the corresponding boundary conditions are

at $z = 0$

$$u^* = w^* = Dw^* = 0; \quad (1-b_l)DT^* = b_l T^*, \tag{54}$$

at $z = 1$

$$Du^* + i\alpha Ma\, T^* = w^* = D^2w^* + i\alpha Du^* + Ma\beta^2 T^* = 0,$$

$$(1-b_u)DT^* = b_u T^*. \tag{55}$$

This set of equations (51)–(55) determines a complex eigenvalue problem for the complex value λ, defined either by

$$\lambda = Ma + is, \tag{56}$$

or

$$\lambda = Ra + is. \tag{57}$$

A particular choice of λ, for instance equation (56), leads to two real characteristic equations from which it is possible to express Ma and s in terms of the remaining parameters

$$Ma = Ma(\alpha, \beta^2, Ra, Pr, b_l, b_u) \tag{58}$$

$$s = s(\alpha, \beta^2, Ra, Pr, b_l, b_u). \tag{59}$$

For given values of Ra, Pr, b_l, b_u, the critical Marangoni number Ma^c is obtained by minimizing equation (58) with respect to both α and β:

$$Ma^c = \min_{\alpha,\beta} Ma(\alpha, \beta^2, Ra, Pr, b_l, b_u) = Ma^c(\alpha^c, \beta^{c2}, Ra, Pr, b_l, b_u). \tag{60}$$

Observe that Ma and s depend on β only through its square value β^2, because of the flow symmetry with regard to the x-axis. From this observation it follows that $\beta_c = 0$ is a privileged value for β.

5. NUMERICAL PROCEDURE

To solve the eigenvalue problem equations (51)–(55) which consists in finding the eigenvalues $\lambda = Ma + is$ (or $\lambda = Ra + is$), we convert it into an inhomogeneous boundary value problem. We impose a priori a λ-value and introduce a normalization condition, selected as $T^*(1) = 1$, which allows us to relax a homogeneous boundary condition, for instance the condition $w^*(0) = 0$. Determining the solution λ of the eigenvalue problem is equivalent to searching the λ-value of the boundary value problem under the condition that $w^*(0) = 0$ is satisfied. The boundary value problem is solved with the D02GBF NAG Fortran Library Routine using a finite-difference method with deferred correction; a general Newton–Raphson algorithm gives the λ-value. Finally the critical λ-value is found by minimizing with respect to the wave numbers α and β. These routines were performed on an IBM 3090 200/E vectorial computer. It should be noticed that CPU times increases rapidly as the Rayleigh and/or the Prandtl numbers become larger and larger.

6. RESULTS

The numerical results have been obtained for a simplified version of the model established in Section 4. Here, we consider a 3-dimensional thin fluid layer of infinite horizontal extent bounded below by an adiabatically isolated rigid plane and above by an adiabatically isolated flat free surface. The fluid layer is subdued to a horizontal gradient of temperature along the upper surface: no vertical temperature gradient is imposed. In addition, a zero-mass flux $M = 0$ through any vertical section is maintained. Under these conditions, the basic velocity profile corresponds to the so-called return flow solution given by equation (20) and represented on Fig. 1. The range of variation of the Prandtl number is selected as $[10^{-2}, 10]$ and positive or zero Marangoni numbers are considered. To summarize,

$$b_l = b_u = 0 \tag{61}$$

$$Q_v = 0, \quad Q_h = 1 \tag{62}$$

$$M = 0 \tag{63}$$

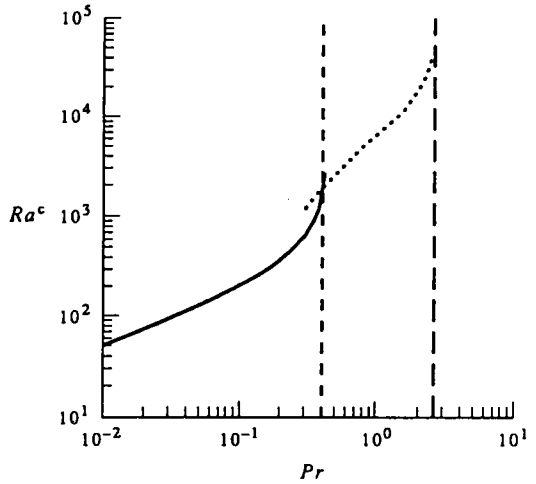

FIG. 2. The critical Rayleigh number Ra^c vs Pr in the pure thermogravitational case; the value $Pr = 0.4$ corresponds to the bifurcation point; the value $Pr = 2.6$ corresponds to the asymptotic value of Ra^c ($Ma = 0$; $b_u = b_l = 0$; $Q_h = 1$; $Q_v = 0$; return flow).

$$Pr \in [10^{-2}, 10] \tag{64}$$

$$Ma \geqslant 0. \tag{65}$$

6.1. *Pure buoyancy instability* ($Ma = 0$)

It is shown that for the return flow the thermoconvective instabilities are taking the form of propagating hydrothermal waves: no stationary instabilities have been displayed. Figures 2 and 3 give the critical Rayleigh and Grashof numbers for Prandtl numbers greater than 10^{-2} up to 10. Two distinct curves which intersect at $Pr = 0.4$ are exhibited. The first one, corresponding to $4 \times 10^{-3} \leqslant Pr \leqslant 0.4$, reproduces the results found by Laure and Roux [5, 12]. On the graph Ra^c vs Pr (Fig. 2), the curve is monotonously increasing with Prandtl number while on the graph Gr^c–Pr (Fig. 3), a minimum is observed at about $Pr \approx 0.2$. The instability threshold of this first mode tends asymptotically to infinity for $Pr \to 0.41$. On Fig. 4, we have reported the angle of propagation of the disturbances vs the Prandtl number. It is shown that for $Pr \to 0.41$. longitudinal rolls corresponding to $\Psi = 90°$, i.e. $\alpha = 0$, are predicted. This confirms previous results by Hart [11] who found that longitudinal rolls are more unstable than transverse ones.

Figure 5 shows that, after a slow increase, the critical wave number k_c becomes smaller and smaller as Pr tends towards the asymptotic value $Pr = 0.41$. From the other side, the phase speed increases monotonously with Pr (Fig. 6). Physically, the instability takes place with larger and larger rolls travelling at greater and greater velocity.

To our knowledge, the instability problem for $Pr > 0.4$, in adiabatically bounded layers, and for $Pr > 1$ under other boundary conditions, has not been treated earlier. Our calculations exhibit the presence of a second instability curve which occurs for $0.4 \leqslant Pr \leqslant 2.6$, with an asymptotic behaviour at $Pr \approx 2.6$. The angle of propagation Ψ for this second mode of instability decreases rapidly from 63° to 0°, which corresponds to transverse rolls ($\beta = 0$) (Fig. 4). The wave number, as well as the phase speed, tends to infinity in the neighborhood of the asymptotic value $Pr = 2.6$. Physically, the instability takes place with smaller and smaller rolls travelling at greater and greater speed.

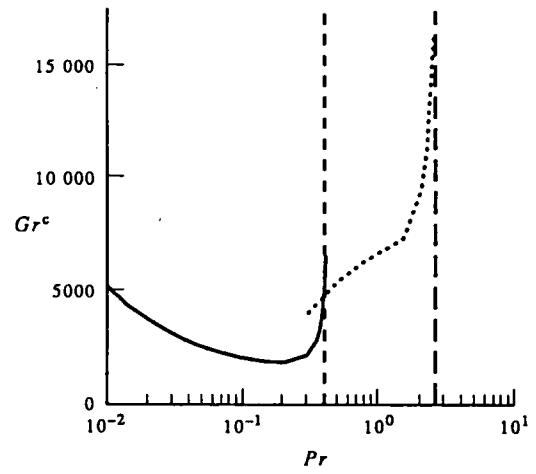

FIG. 3. The critical Grashof number Gr^c vs Pr in the pure thermogravitational case; the vertical dashed line at $Pr = 0.4$ corresponds to the bifurcation point; the vertical dashed line at $Pr = 2.6$ corresponds to the asymptotic value of Gr^c ($Ma = 0$; $b_u = b_l = 0$; $Q_h = 1$; $Q_v = 0$; return flow).

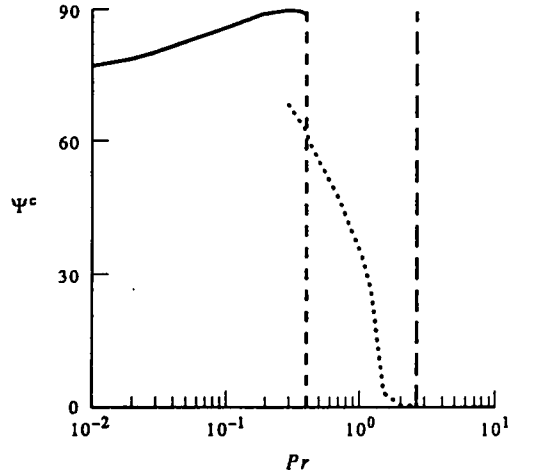

FIG. 4. Angle of propagation Ψ^c of the disturbance vs Pr in the pure thermogravitational case; the vertical dashed lines at $Pr = 0.4$ and 2.6 correspond to the bifurcation point and the asymptotic value of Ra^c respectively ($Ma = 0$; $b_u = b_l = 0$; $Q_h = 1$; $Q_v = 0$; return flow).

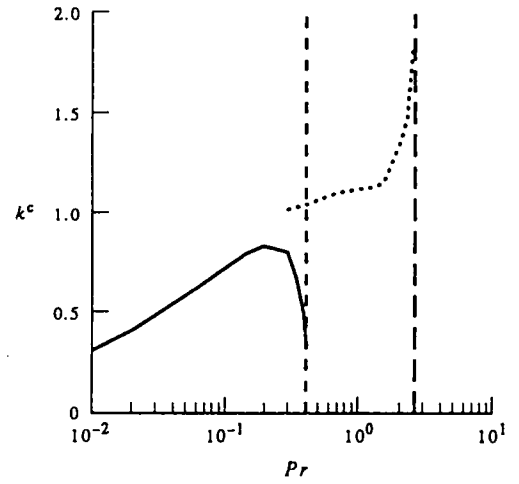

FIG. 5. The critical wavenumber k^c vs Pr in the pure thermogravitational case ($Ma = 0$; $b_u = b_l = 0$; $Q_h = 1$; $Q_c = 0$; return flow).

For $Pr > 2.6$, no critical Rayleigh number is found. To check this result, an independent numerical experience was performed. A bidimensional finite-difference program was used in the case of a layer with $Pr = 7$ confined in a rectangular box of aspect ratio $A(=l/d) = 4$, with adiabatically isolated horizontal boundaries and perfectly conducting vertical walls: the calculations were performed for Ra values up to 10^7. The result was edifying: no transverse roll was exhibited confirming that the situation is unconditionally stable. It should also be noticed that because of the 2-dimensionality of the numerical scheme, only transverse rolls are allowable.

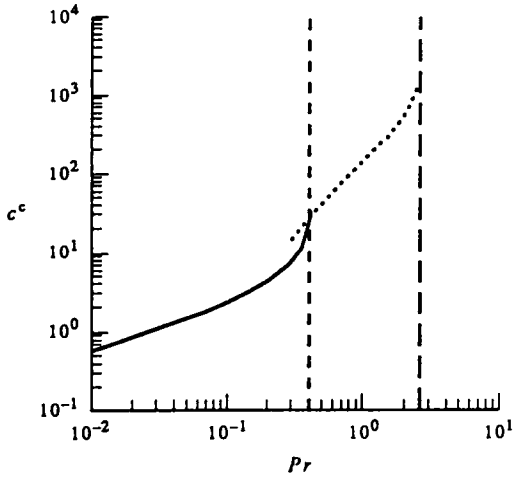

FIG. 6. The critical phase speed c^c vs Pr in the pure thermogravitational case ($Ma = 0$; $b_u = b_l = 0$; $Q_h = 1$; $Q_c = 0$; return flow).

Figure 2 can also be exploited to show the influence of the viscosity on the stability of the basic state. Consider two fluids with the same thickness, say fluid$^{(1)}$ and fluid$^{(2)}$, whose physical parameters are identical except for the viscosity and suppose $\mu^{(1)} < \mu^{(2)}$, so that $Pr^{(1)} < Pr^{(2)}$. From Fig. 2, it is found that $Ra^{(1)c} < Ra^{(2)c}$, from which follows that $\beta_T^{(1)c} < \beta_T^{(2)c}$: this result is in agreement with the physically intuitive conclusion that the more viscous is the fluid, the more stable is the flow.

Figure 3 gives some hints on the influence of thermal conductivity on the stability of the basic state. Like above, consider two identical fluids with the same thickness, except for thermal conductivity, and suppose $K^{(1)} > K^{(2)}$. If the corresponding Prandtl numbers are in the range $4 \times 10^{-3} \leqslant Pr^{(1)} < Pr^{(2)} \leqslant 0.2$, it is observed on Fig. 3 that $\beta_T^{(1)c} > \beta_T^{(2)c}$; it can thus be said that stability is increased when the heat conductivity becomes larger and larger. For Prandtl numbers in the range $0.2 \leqslant Pr^{(1)} < Pr^{(2)} \leqslant 2.6$, by decreasing the conductivity one reinforces the stability. It follows from the results reported on Fig. 3 that for a given set μ, C_p and ρ_0, there exists a critical conductivity given by $K_c = 5\mu C_p \rho_0^{-1}$ at which the basic state is the most unstable.

In summary, it has been shown that buoyancy instabilities appear only under the form of travelling rolls for Prandtl numbers smaller than 2.6; above this limit, our results indicate that the flow is stable with respect to buoyancy disturbances. The angle of propagation, the wavelength and the perturbation phase speed depend strongly on the Prandtl number. The perturbation can appear either under the form of nearly longitudinal rolls ($\alpha \approx 0$) for $Pr < 0.4$ or under the form of transverse rolls ($\beta = 0$) for $Pr \geqslant 2$, either with relatively long wavelengths (for $Pr < 0.4$) or short wavelengths (for $Pr > 0.4$), with large phase speed (at $Pr \approx 2.6$) or small phase speed (at $Pr \approx 10^{-2}$). This wide diversity of results leads to the impossibility to draw a general conclusion on the behaviour of travelling disturbances when buoyancy is the single motor of instability.

6.2. *Coupled buoyancy and thermocapillary* ($Ma \neq 0$, $Ra \neq 0$)

We now discuss the coupling of the buoyancy and surface-tension driven instabilities. The pure Marangoni problem, without buoyancy effect, was treated by Smith and Davis [6] and therefore will not be repeated here.

The present analysis considers five different values of the Prandtl number, namely $Pr = 10^{-2}$, 10^{-1}, 1, 3 and 7. The instability thresholds are represented on Rayleigh–Marangoni and Grashof–Reynolds graphs as they bring interesting complementary informations. The other results (phase speed, wave number, angle of propagation) will be represented as a function of the Rayleigh number.

The results display three kinds of behaviour according to the values taken by the Prandtl number: the

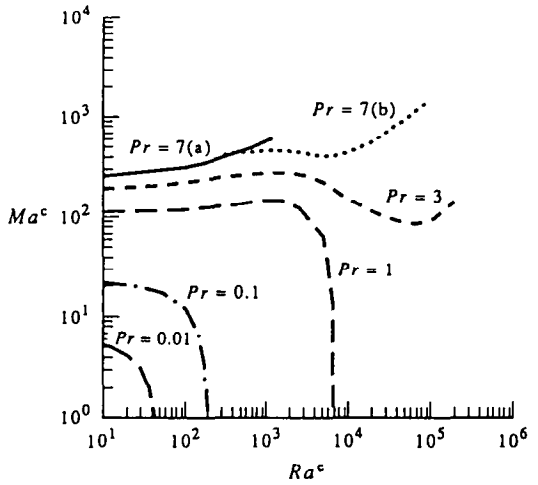

FIG. 7. The critical Marangoni number Ma^c vs the critical Rayleigh number Ra^c at five different Prandtl numbers ($Pr = 10^{-2}, 10^{-1}, 1, 3, 7$). The curve $Pr = 7$ is composed of two distinct solutions (a) and (b), which intersect at $Ra^c = 365$ ($b_u = b_l = 0$; $Q_h = 1$; $Q_c = 0$; return flow).

first one, $4 \times 10^{-3} \leqslant Pr \leqslant 0.4$, will be referred to as the 'a-family'; the second one, $0.4 \leqslant Pr \leqslant 2.6$ as the 'b-family' and the third one, $Pr \geqslant 2.6$, as the 'c-family'.

Figures 7 and 8 give the critical values in both the Ra^c–Ma^c and Gr^c–Re^c representations. It must be realized that both representations describe the same physical situation, but that in some circumstances the effects are better described on one graph rather than on the other.

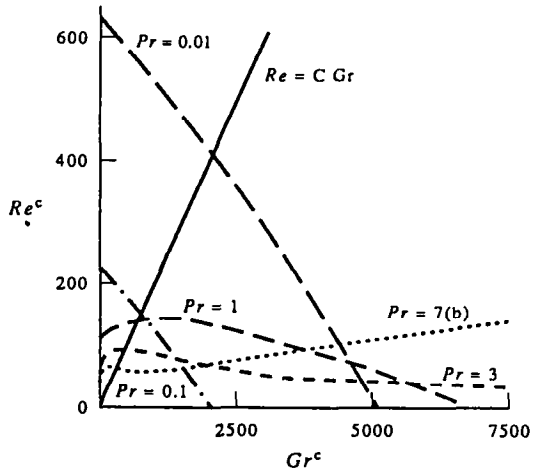

FIG. 8. The critical Reynolds number Re^c vs the critical Grashof number Gr^c at five different Prandtl numbers ($Pr = 10^{-2}, 10^{-1}, 1, 3, 7$). In this linear scale, only the second part (b) of the curve $Pr = 7$ is represented. The straight line $Re = C\ Gr$ gives the couple of values Re–Gr corresponding to a given fluid with a given depth ($b_u = b_l = 0$; $Q_h = 1$; $Q_c = 0$; return flow).

Concerning the a-family (curves $Pr = 10^{-2}$ and 10^{-1}), it is seen that at a fixed value of Pr, Ma^c (Re^c) decreases monotonously with Ra^c (Gr^c) indicating that both buoyancy and thermocapillarity effects are tightly coupled. It follows from Fig. 8 that the relation $Re^c = f(Gr^c)$ can be approximated by the linear law $Gr^c/Gr_0^c + Re^c/Re_0^c = 1$ or, after simplification by Pr, $Ma^c/Ma_0^c + Ra^c/Ra_0^c = 1$; the quantities Ma_0^c (Re_0^c) and Ra_0^c (Gr_0^c) are the Ma^c (Re^c) and Ra^c (Gr^c) values corresponding to pure surface tension driven and pure buoyancy instability respectively. This result shows that at small Pr values, buoyancy and capillary effects are strongly-tied. Note that this relation is reminiscent of the straight line found by Nield [1] for a fluid, at rest in the basic state, heated from below.

Stability can be discussed from two different points of view: either by analysing the effects of variation of a dimensionless parameter on the behaviour of other characteristic numbers, or by examining the stabilizing effects of a relevant physical parameter, like the imposed temperature gradient. As illustration of the first point of view, it is noted that an increase of Pr raises the critical values Ma^c and Ra^c while an increase of Pr has the opposite effect on the critical Gr^c and Re^c numbers, which decrease with Pr. The most interesting physical insight provided by the second point of view will be discussed in Section 6.3.

The curves describing the a-family ($Pr = 10^{-2}$ and 10^{-1}) and the b-family ($Pr = 1$) intersect the coordinates axis $Ra^c = 0$ (respectively $Gr^c = 0$ and $Re^c = 0$): the differences between these two families is that the curves of the b-family pass through a maximum. The c-family curves are characterized by unconditional stability in the case of pure buoyancy since they do not cut the Ra^c (respectively, Gr^c) axis. The curves for $Pr = 3$ and 7 admit two extrema with a weak dependence of Ma^c vs Ra^c (respectively, Re^c vs Gr^c). In the last parts of these curves ($Ra^c > 7 \times 10^3$ ($Gr^c > 10^3$) for $Pr = 7$ and $Ra^c > 5 \times 10^4$ ($Gr^c > 1.67 \times 10^4$) for $Pr = 3$, Ma^c (Re^c) increases monotonously with Ra^c (Gr^c) with a weak dependence of Ma^c vs Ra^c, indicating that buoyancy and thermocapillarity are loosely tied. It is also worth noticing that the curve $Pr = 7$ exhibits a bifurcation at $Ra^c = 365$ ($Gr^c = 52$).

Figures 9–11 represent respectively the wave number, the angle of propagation and the phase speed of the perturbation vs the Rayleigh number. Concerning the a-family it is noted that the wave number and phase speed are particularly unaffected by the presence of the buoyancy effect, while the direction of propagation of rolls remains close to that of the basic flow. In contrast, in the case of the c-family, the travelling rolls become transverse from large Ra values; a substantial increase of the wave number and phase speed is also observed after that Ψ^c is equal to zero, i.e. for transverse rolls. In the particular case $Pr = 7$ and $Ra = 365$, at which bifurcation occurs, the rolls undergo a radical change in their behaviour, this is particularly true for the angle of propagation. Finally,

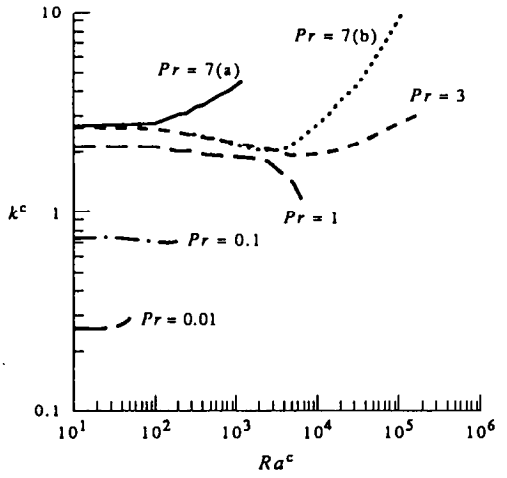

FIG. 9. Critical wavenumber k^c vs critical Rayleigh number Ra^c at five different Prandtl numbers ($Pr = 10^{-2}, 10^{-1}, 1, 3, 7$) ($b_u = b_l = 0$; $Q_h = 1$; $Q_r = 0$; return flow).

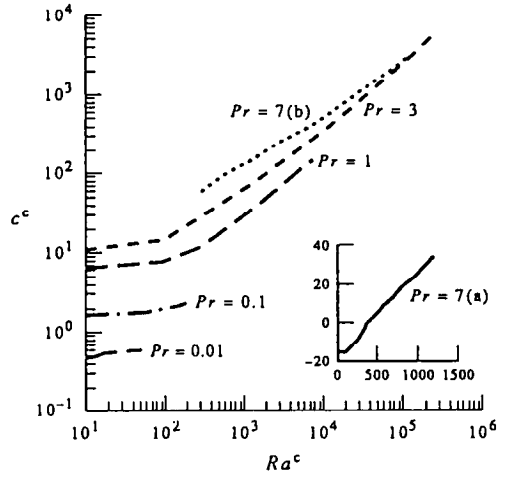

FIG. 11. Critical phase speed c^c vs critical Rayleigh number Ra^c at five different Prandtl numbers ($Pr = 10^{-2}, 10^{-1}, 1, 3, 7$) ($b_u = b_l = 0$; $Q_h = -1$; $Q_r = 0$; return flow).

the trend of the b-family curves is seen to be intermediate between these of the a- and c-families.

6.3. *Further comments*

For a given fluid with given depth, the only physical parameter under control is the horizontal temperature gradient β_T. The information obtained from the variations of some quantities like Ma, Gr, ... in terms of the Prandtl number are not directly useful from a practical point of view. Indeed, for a given value of Pr, infinite values of the couple μ (viscosity)–κ (heat diffusivity) are allowable: moreover, we need the knowledge of μ and κ to determine the critical value of the temperature gradient since Ma^c, Ra^c, Gr^c and Re^c depend explicitly on them.

After elimination of β_T between the definitions of Ma and Ra, one obtains a linear relation $Ma^c = C\,Ra^c$ between Ma^c and Ra^c with C given by

$$C = \gamma \rho_0^{-1} \alpha_T^{-1} g^{-1} d^{-2}.$$

The slope of the straight line $Ma^c = C\,Ra^c$ is fixed for a given fluid with a given depth. Of course a similar linear relation $Re^c = C\,Gr^c$ is obtained from the Gr and Re definitions. The intersection of this straight line with the Ma^c–Ra^c (or Re^c–Gr^c) curves gives the Ma^c–Ra^c (respectively, the Re^c–Gr^c) values corresponding to the instability thresholds for a given fluid at a given depth. The corresponding critical temperature gradient β_T is then directly derived from the very definition of the various parameters.

Consider now two fluid layers of same depth with the same physical constants except for the viscosity; assume that $\mu^{(1)} < \mu^{(2)}$ from which it follows that $Pr^{(1)} < Pr^{(2)}$. According to Fig. 7, it is seen that the Marangoni number as well as the Rayleigh number for the fluid 1 is smaller than for fluid 2, from which is directly inferred that

$$\beta_T^{(1)c} < \beta_T^{(2)c}.$$

It is thus concluded that the more viscous the fluid, the more stable the flow; the viscosity thus plays a stabilizing role whatever the values of the physical properties of the fluid.

To study the role of the thermal conduction upon the onset of instability, let us examine Fig. 8. We still consider two fluids differing only by their thermal conductivity and suppose that $K^{(1)} > K^{(2)}$. We

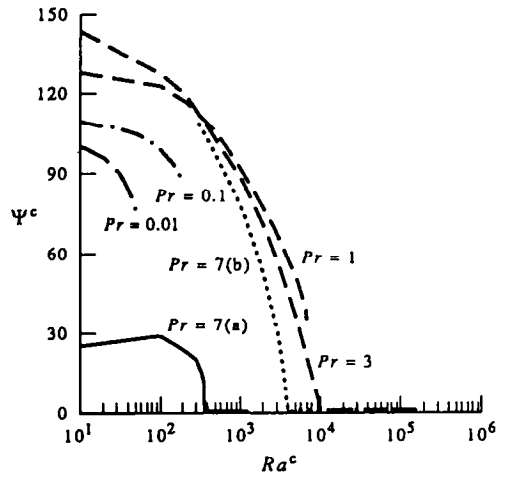

FIG. 10. Angle of propagation Ψ^c of the disturbance vs critical Rayleigh number, Ra^c at five different Prandtl numbers ($Pr = 10^{-2}, 10^{-1}, 1, 3, 7$); the travelling rolls are transverse at $Pr = 3$ for $Ra^c > 10^4$ and at $Pr = 7$ for $335 < Ra^c < 365$ and $Ra^c > 4 \times 10^3$ ($b_u = b_l = 0$; $Q_h = 1$; $Q_r = 0$; return flow).

observe on Fig. 8 that for large C values, which correspond to very thin layers or a microgravity environment, one has

$$Gr^{(1)c} > Gr^{(2)c}$$

or equivalently

$$\beta_T^{(1)c} > \beta_T^{(2)c}.$$

This means that for large C-values, the thermal conductivity is stabilizing. In the opposite case of very small values of C, which corresponds to thick layers wherein buoyancy effects are dominant, we recover the conclusions of Section 6.1, accordingly stability is reinforced when the heat conductivity is increased. However, for intermediate thicknesses, no general rule about the effect of heat conductivity on the onset of instability can be formulated.

Figure 10 shows that at very small Prandtl numbers, the preferred mode of propagation of the hydrothermal waves is nearly longitudinal as Ψ^c is close to 90°. When Pr is increased ($Pr \geqslant 3$) a tendency towards transverse rolls is observed. For these values of Pr, pure transverse rolls ($\Psi^c = 0$) are predicted above a critical value of the Rayleigh number: this value diminishes when Pr increases. In the particular case of pure Marangoni effect ($Ra = 0$), oblique hydrothermal waves are found with a trend towards longitudinal waves at small values of Pr: this result is in agreement with earlier calculations by Smith and Davis [6]. It is also seen on Fig. 10 that for $Pr > 1$ and microgravity conditions ($Ra = 0$), instability takes place as rolls propagating in an oblique direction with respect to the flow; in contrast on earth, where buoyancy effects are dominant (large Ra-values), the preferred mode of propagation is essentially transverse rolls.

Experiments for coupled buoyancy and thermocapillary flows submitted to a horizontal temperature gradient in rectangular boxes were performed by Villers and Platten [4]. These authors worked with acetone whose Prandtl number is 4.24. They observed stationary and oscillatory regimes according to the relative values of the Ra and Ma numbers. We did not calculate the curve for $Pr = 4.24$ as its behaviour is very similar to these obtained for $Pr = 3$ and 7, and because a quantitative comparison with experimental results is not significative, as explained below. For a given Rayleigh number, it is observed that the ratio between the theoretical and experimental Marangoni numbers take values between 10 and 20. This relatively large difference may, from one side, be explained by the presence of the vertical rolls which play a stabilizing role, and which were observed in experiments due to the presence of the lateral walls; moreover the thermal boundary conditions imposed at the horizontal surfaces are different in Villers–Platten's experiments and in our theoretical approach; finally, it is clear that the experimental determination of the critical point is a very delicate task and may be a source of experimental errors. Despite differences between theoretical and experimental predictions, it must be emphasized that experiments confirm the presence of travelling waves and the general trend that, at large Ra^c-values, Ma^c is increasing with Ra^c. Clearly, more experimental data on boxes with various aspect ratios will be welcomed.

7. SUMMARY AND FINAL REMARKS

The aim of this work was to examine the problem of coupled buoyancy and thermocapillary driven convection in thin fluid layers of lateral infinite extent submitted to a horizontal temperature gradient. In contrast with the classical Bénard–Marangoni convection in a layer heated from below, the basic reference state is no longer a quiescent state but the imposed temperature gradient generates instantaneously a fluid flow: in the present work the resulting basic velocity profile has been supposed to take the form of a return flow solution. The linear stability of the basic flow is analysed by superimposing a three-dimensional disturbance and applying the normal mode technique. It was shown that the resulting disturbances take the form of rolls propagating generally in an oblique direction with regard to the basic flow. Steady perturbations were not predicted.

The main results and original contributions of the present work can be summarized as follows:

(1) the basic flow equations have been formulated under rather general conditions with an imposed temperature gradient arbitrarily oriented. Up to now, either vertical or horizontal temperature gradients were considered;

(2) our linear stability analysis is complementary to recent contributions by Smith and Davis [6] and Ben Hadid *et al.* [8]. The first authors restrict their analysis to the pure Marangoni problem while the second authors consider coupled buoyancy and surface-tensions driven flows: however, they restrict their analysis to low Prandtl number ($Pr < 1$); moreover, Ben Hadid *et al.* [8] use different boundary conditions for the basic and the perturbated flows and therefore their results cannot be compared either with ref. [6] or with the present ones;

(3) in pure thermocapillary convection ($Ra = 0$), our results are in excellent quantitative agreement with Smith and Davis [6]. In pure buoyancy-driven flow ($Ma = 0$) our results are identical to those of Laure and Roux [12] who explore the Pr-region between 4×10^{-3} and 0.4. The case of coupled buoyancy and thermocapillary effects was treated by Ben Hadid *et al.* [8, 10] but only for small values of the Prandtl number. However, as explained earlier, their results are not comparable with ours because of their particular choice of boundary conditions;

(4) it was found that the behaviour of the system is widely dependent on the Pr-values. This has motivated the introduction of three different Pr-families: the a-family corresponds to very small values of Pr

($4 \times 10^{-3} < Pr < 0.4$), the b-family runs from $Pr = 0.4$ to 2.6 while the c-family describes systems for $Pr > 2.6$. In this later case, a bifurcation at $Pr = 7$ and $Ra^c = 365$ is displayed;

(5) perturbations in the form of propagating transverse rolls ($\Psi = 0$) are favored when buoyancy forces are dominating, whereas nearly longitudinal waves ($\Psi \approx 90^\circ$) are preferred under microgravity conditions and small Prandtl numbers;

(6) whatever the value of the Prandtl number, viscosity always plays a stabilizing role; no general conclusion can be drawn about the influence of the heat conductivity on the stability of the flow;

(7) it was shown by Nield [1] that for cells heated from below, buoyancy has a destabilizing effect. In the case of an imposed horizontal temperature gradient, this is only guaranteed for Pr-values larger than 2.6; nevertheless for Prandtl numbers smaller than 0.4 and large Ra values, buoyancy is also stabilizing as confirmed by the experimental work of Villers and Platten [4]; and

(8) as noticed at the end of the last section, comparison with experiments seems to confirm the general trends of our theoretical approach. Of course, a more decisive comparison with experiments would require a greater number of experimental data and a refinement of the model presented here by including lateral boundary conditions and examining the role of other basic velocity profiles than the return flow; it would also be interesting to discuss the influence of an inclined temperature gradient.

Acknowledgements—Fruitful discussions with Prof. J. K. Platten and his group (Mons University) are acknowledged. This text presents research results of the Belgian programme on Interuniversity Poles of attraction (PAI no. 29) initiated by the Belgian State, Prime Ministers Office, Science Policy Programming. The scientific responsibility is assumed by its authors.

REFERENCES

1. D. A. Nield, Surface tension and buoyancy effects in cellular convection, *J. Fluid Mech.* **19,** 341–352 (1964).
2. A. G. Kirdyashkin, Thermogravitational and thermocapillary flows in a horizontal liquid layer under the conditions of a horizontal temperature gradient, *Int. J. Heat Mass Transfer* **27,** 1205–1218 (1984).
3. D. Villers and J. K. Platten, Influence of thermocapillarity on the oscillatory convection in low *Pr* fluids, *Notes on Numerical Fluid Mechanics*, Vol. 27, pp. 108–116. Vieweg, Braunschweig (1990).
4. D. Villers and J. K. Platten, Coupled buoyancy and Marangoni convection in acetone: experiments and comparison with numerical simulations, *J. Fluid Mech.* **234,** 487–510 (1992).
5. P. Laure and B. Roux, Numerical simulation of oscillatory convection in low-*Pr* fluids. Linear and non linear analysis of the Hadley circulation. In *Notes on Numerical Fluid Mechanics*, Vol. 27, pp. 307–318. Vieweg, Braunschweig (1990).
6. M. K. Smith and S. H. Davis, Instabilities of dynamic thermocapillary liquid layers. Part 1. Convective instabilities, *J. Fluid Mech.* **132,** 119–144 (1983).
7. M. K. Smith and S. H. Davis, Instabilities of dynamic thermocapillary liquid layers. Part 2. Surface-wave instabilities, *J. Fluid Mech.* **132,** 145–162 (1983).
8. H. Ben Hadid, B. Roux and P. Laure, Thermocapillarity effects on the stability of buoyancy-driven flows in shallow cavities, *PhysicoChem. Hydrodyn.* **11,** 625–644 (1989).
9. A. Cloot and G. Lebon, Marangoni instability in a fluid layer with variable viscosity and free interface, in microgravity, *PhysicoChem. Hydrodyn.* **6,** 453–462 (1985).
10. H. Hadid and B. Roux, Buoyancy- and thermocapillary-driven flows differentially heated cavities for low-Prandtl-number fluids, *J. Fluid Mech.* **235,** 1–36 (1992).
11. J. Hart, A note on stability of low-Prandtl-number; Hadley circulations, *J. Fluid Mech.* **132,** 271–281 (1983).
12. P. Laure and B. Roux, Synthèse des résultats obtenus par l'étude de stabilité des mouvements de convection dans une cavité horizontale de grande extension, *C. R. Acad. Sci. Paris II* **305,** 1137–1143 (1987).
13. A. K. Sen and S. H. Davis, Steady thermocapillary flows in two-dimensional slots, *J. Fluid Mech.* **121,** 163–186 (1982).